International Journal of
Plasma Environmental Science and Technology

Regular Paper (***Special Issue* of ICESP2024**) DOI: 10.34343/ijpest.2025.19.e02012

A study on the measurement of charge and surface potential of charged liquid droplets in spray painting

Rito Jin[1], Yuta Kurihara[1], Masatoshi Daikoku[1,*], Minori Shirota[2]
Taimei Miyagawa[2], Takahiro Okabe[2], Yoshiya Matsukawa[3], Hideyuki Aoki[3]
Yasuhiro Saito[4], Junichi Fukuno[5]

[1] Hachinohe Institute of Technology, Japan
[2] Hirosaki University, Japan
[3] Tohoku University, Japan
[4] Kyushu Institute of Technology, Japan
[5] Honda Motor Co., Ltd., Japan

* Corresponding author: aikoku@hi-tech.ac.jp (Masatoshi Daikoku)

Received: 27 December 2024
Revised: 18 February 2025
Accepted: 18 March 2025
Published online: 28 March 2025

Abstract
The charge and surface potential of liquid droplets falling from a nozzle were measured in order to clarify the charging and discharging properties of droplets formed under an applied voltage during automotive spray painting. The charge per droplet was found to initially increase with increasing voltage regardless of the test liquid used but then began to decrease due to a reduction in droplet size, the generation of satellite droplets, and electrical discharging. The 'electrical surface tension' was also determined and was found to be nondimensionally correlated with the surface charge density. The surface potential for moving droplets, stationary metallic disks, and spheres was measured using an electrostatic sensor, whose principles were applied in an attempt to correct the displayed values based on the size of the droplets. A regression analysis was also used to correct the displayed surface potentials. It was found that accurate measurement of the surface potential may be possible even for small particles.

Keywords: Charge, surface potential, liquid droplets, spray painting.

1. Introduction

During automotive spray painting, around 30% of the paint does not reach the car body and is wasted. As the painting process consumes 25 to 40% of the total energy required to manufacture a car, it is therefore desirable to increase the paint-transfer efficiency. Currently, high-speed rotary bell-cup atomizers are used in automotive spray painting, and extensive research has been conducted on the painting process. This process consists of three stages: atomization, flight and deposition of spray droplets, and film formation.

Ogasawara *et al*. investigated the atomization process and classified the dependence of the liquid film-flow patterns on the surface of a rotary bell cup on the rotational speed and liquid flow rate and investigated the influence of these patterns on the breakup at the bell-cup edge [1]. Soma et al. simulated liquid-film formation on the bell-cup surface under painting conditions using the volume-of-fluid method and elucidated the hydrodynamic behavior of a liquid film flowing on a rotary bell-cup surface [2]. Hatayama *et al*. experimentally observed the breakup process for liquid filaments generated at the grooved edge of a high-speed rotary bell-cup atomizer and quantitatively evaluated the filament diameter and length using image processing. They demonstrated that the droplet size distribution normalized by the arithmetic mean diameter could be well represented by a gamma distribution [3]. Sawaguchi *et al*. conducted an experiment to reproduce a liquid filament from a groove at a bell-cup edge by ejecting liquid from a nozzle and impinging it with a

high-velocity airflow (shaping air) from a slit nozzle. Based on these results, they nondimensionalized the spray angle using the Reynolds number and the mean droplet diameter using the Weber number [4].

Recently, many studies have used computational fluid dynamics to investigate droplet behavior in high-speed rotary bell-cup atomizers, which is difficult to measure experimentally. Matsushita et al. analyzed the spray flow in a rotary bell-cup atomizer using a large eddy simulation and k-ε two-equation model, evaluated the accuracy of the analysis, and reported the effect of the turbulence model on spray particle behavior [5]. However, the atomization process, which involves droplet charging under a high applied voltage, is highly complex and has not yet been fully elucidated or modeled.

Our recent research on painting processes has shifted toward the flight and deposition of spray droplets and film formation, increasingly under conditions involving electrostatic charging using a high applied voltage. To investigate the flight and deposition processes for spray droplets, Yasumura *et al*. simulated the spray flow around a high-speed rotary bell cup and compared the results with those obtained by particle image velocimetry measurements, identifying factors that reduce the transfer efficiency and clarifying the effects of the shaped air and applied voltage on droplet behavior [6].

To investigate film formation on a car body, Shirai *et al*. studied the impact of charged droplets on a transparent conductive substrate. They investigated the influence of droplet charge on the shape of the dimple formed just before impact and the size and number density distribution for air bubbles captured upon impact [7]. Furthermore, Kodama *et al*. conducted a study on droplet impact on a liquid film. They determined the time variation of the contact line velocity when an air film with a thickness of approximately 100 nm was present during the droplet spreading process [8]. However, many aspects of the charging and discharging characteristics of paint droplets remain unclear [9].

Our final goal is to elucidate the charging mechanism for droplets generated from liquid filaments at the bell cup under a high applied voltage, which will enable us to improve the accuracy of simulations for electrostatic spray painting in automotive manufacturing. It is thus crucial to accurately estimate the charge per droplet and the droplet diameter for use as initial conditions for the simulation. Seike measured the total charge for a spray generated by high-pressure injection of ultrapure water to establish electrostatic discharge prevention technology for semiconductor device cleaning processes [10]. Additionally, while Tabata *et al*. and Endo have reported on the charge per unit mass or per spray duration for liquids [11−13], there have no reports on the charge per droplet under a high applied voltage.

Therefore, the objective of this study is to investigate the influence of the geometry of a test object on the results of surface potential measurements. This will allow us to measure the charge and surface potential of a liquid droplet to clarify the basic characteristics of electrification during spraying.

2. Experimental setup and conditions

2.1 Measurement of charge of droplets

Fig. 1 shows the equipment used to measure the charge and surface potential of liquid droplets. A syringe pump was used to continuously supply liquid (12 mL h^{-1}) to the nozzle (outer diameter D = 1.25 mm, length 80 mm). Charged liquid droplets were formed during this time by applying a negative voltage to the nozzle using a negative polarity high-voltage power supply (HVU-30N100, MECC Co., Ltd.). The droplets entered a Faraday cage (KQ-1400, Kasuga Electric Works, Ltd.) and the charge was measured using an electrometer (8252, ADC Corporation). In this experiment, the distance from the nozzle tip to the Faraday cage was 80 mm, and the entrance of the Faraday cage was a circular hole with a diameter of 10 mm. The optimal diameter of the entrance was determined through preliminary experiments in order to make the electrometer readings stable and allow the main droplets to enter the Faraday cage. A high-voltage meter (149-10A, Kikusui Electronics Corporation) was used to accurately measure the applied voltage. The breakup behavior of the liquid was captured using an INFINICAM high-speed camera (Photron, Ltd.) at 1000 to 1500 fps, and the droplet shape and electrical discharge phenomena were captured with a still camera (PENTAX K-7). The droplet shape was captured at ISO 250 with a shutter speed of 1/125 s, while the electrical discharge phenomena were captured at ISO 1600 with a 30 s exposure time. The diameter of the droplets was calculated from the flow rate (12 mL h^{-1}) and the formation cycle time. Water, ethanol, glycerin, and an ethanol/glycerin mixture as a pseudo paint were used as the test liquids.

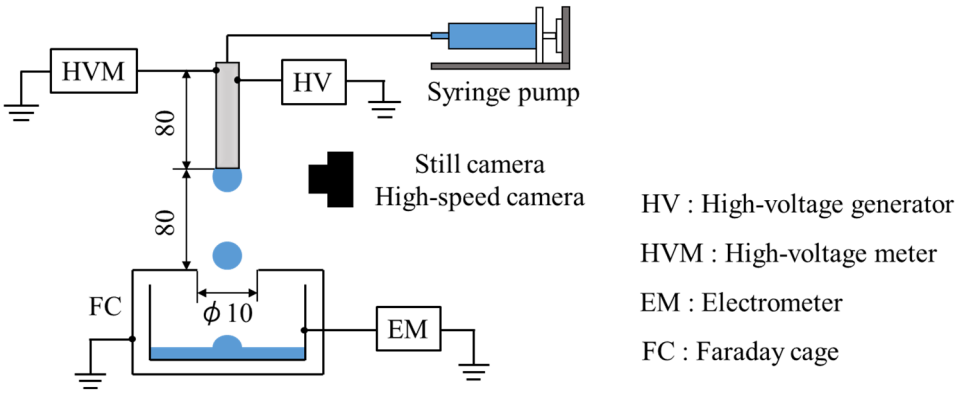

Fig. 1. Measurement system for charge and surface charge density.

Table 1 shows the physical properties [14−17] of the test liquids used in this study. The surface tension, viscosity, and density of the liquid were confirmed through experiments, while the electrical conductivity was obtained from the literature [16, 17]. In general, water is initially used in atomization research, and the experimental results are used for comparison with other test liquids. It is also well known that physical properties such as surface tension and viscosity significantly affect the atomization characteristics [18]. Therefore, ethanol was used to investigate the effect of surface tension, and glycerin was used to investigate the effect of viscosity. An ethanol/glycerin mixture with a concentration ratio of 30:70 (wt%) is used in the present study as a pseudo paint [8] because its physical properties are similar to those of the paint used in automotive factories.

Table 1. Physical properties of test liquids [8, 14−17].

Liquid	μ_L [mPas]	γ_L [mN m^{-1}]	ρ_L [kg m^{-3}]	κ_L※ [S m^{-1}]
Distilled water	1.002	72.6	998.2	1×10^{-4}
Ethanol 100 wt%	1.2	22.4	789.2	1.35×10^{-7}
Glycerin 100wt%	1410	62.8	1261.1	6.4×10^{-6}
Pseudo paint Ethanol/Glycerin 30:70 (wt%)	64	50	1082	–

※ Reported electrical conductivity [16, 17]

2.2 Measurement of surface potential

One of the objectives in this study is to measure the surface potential of small liquid droplets, but the electrostatic sensor used for the experiments measures the surface potential of a bigger plane than the originally predetermined dimensions (20 mm). In preliminary tests, we attempted to measure the surface potential of moving droplets, but due to the influence of their small size and velocity, the values displayed by the sensor were only around 1/16th of the applied voltage [9].

For this reason, we first analyzed the characteristics of the electrostatic sensor using a stationary calibration disk (radius $b_0 = 10$ mm). Subsequently, we measured the surface potential of disks smaller than the calibration disk and applied corrections based on the measurement principle of the electrostatic sensor. In addition, since the liquid droplets we wish to measure are assumed to be spherical, we investigated the influence of the shape of the measured test object on the displayed surface potential values. To this end, we measured the surface potential of a stationary metallic sphere and applied corrections to the displayed surface potential values in the same manner as for the disk.

Fig. 2 (a) shows the setup for measuring the surface potential of a disk and a sphere, both of which were fixed with a metallic rod attached to their rear surface, together with the coordinate system used shown in Fig. 2(b). The disk (radius b = 2.5−15 mm) and sphere (radius R = 1.0−15 mm) were charged using a high-

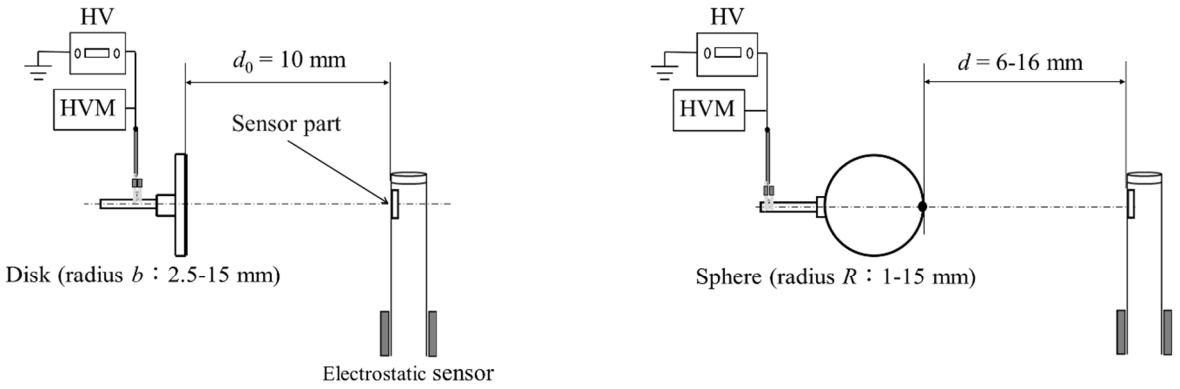

(a) Surface potential measurement system for disk and sphere

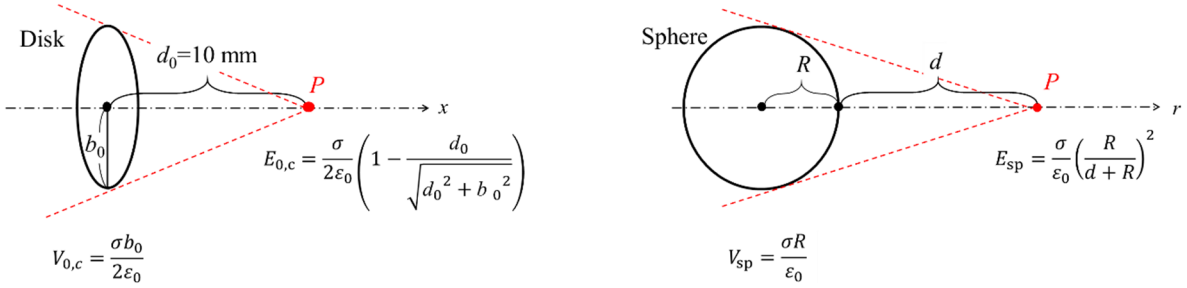

(b) Coordinate system for disk and sphere

Fig. 2. Surface potential measurement system for disk and sphere.

voltage power supply, and an electrostatic sensor (KSD-3000 digital low potential measuring device, Kasuga) was used to measure the surface potential. To investigate the influence of the disk size, experiments were conducted by varying the disk radius from 2.5 to 15 mm. To investigate the influence of the distance between the sphere surface and the sensor, experiments were conducted by varying the sphere-sensor distance from 6 to 16 mm. The applied voltage used for all experiments was 500 V.

3. Measurement of charge

Fig. 3 (a) shows the variation of the charge per droplet Q on the applied voltage for water, 100 wt% ethanol, and 100 wt% glycerin. In each case, the charge initially increases as the applied voltage is increased and then begins to decrease at a certain voltage that depends on the liquid used. This is thought to be due to a reduction in droplet size as well as the generation of satellite droplets and discharge from the droplets as the applied voltage is increased. Discharge from the water droplets was confirmed by photography [9]. The significantly lower charge for 100 wt% ethanol is due to the low surface tension of ethanol, which results in a smaller droplet size. Although the surface potential of glycerin is not significantly different from that of water, as the applied voltage is increased, the charge on glycerin droplets is seen to become smaller than that on water droplets. This is thought to be due to the viscosity of glycerin, which is about 1400 times larger than that of water at room temperature. Under a high voltage, this causes the formation of long, fine ethanol filaments, which are observed to scatter as fine satellite droplets, resulting in a lower droplet charge.

Fig. 3 (b) shows the variation of the droplet diameter d_p on the applied voltage. Regardless of the test liquid, the droplet diameter is seen to decrease with increasing voltage. This is considered to be due to an increase in the electrostatic force acting on the droplet as the applied voltage is increased, which causes the smaller droplet to be pulled downward. For the same applied voltage, the smallest droplets are observed for 100 wt% ethanol, followed by 100 wt% glycerin, with water exhibiting the largest droplet diameter. This is a similar trend to that for the surface tension, and indicates that a liquid with a high surface tension produces larger droplets.

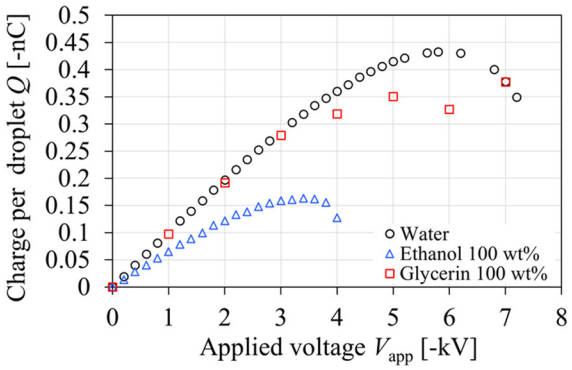

(a) The variation of charge with applied voltage

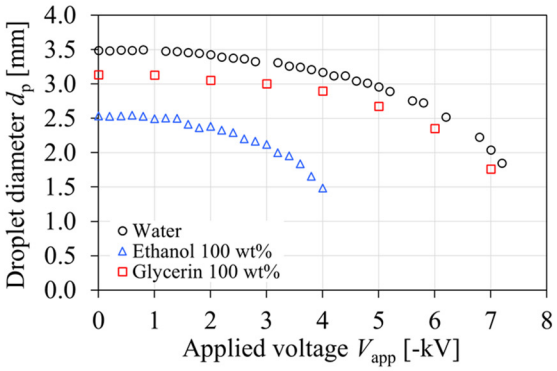

(b) The variation of droplet diameter with applied voltage

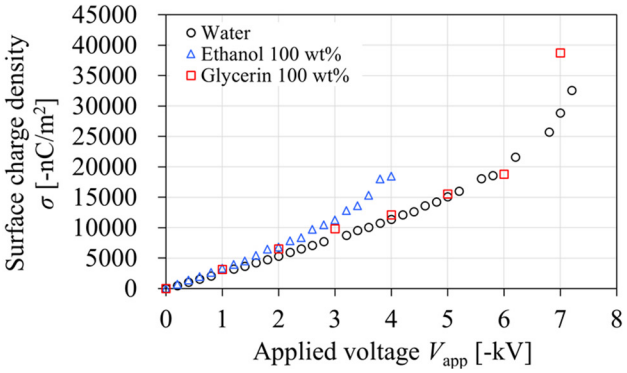

(c) The variation of surface charge density with applied voltage

Fig. 3. The variation of charge per droplet, droplet diameter and surface charge density with applied voltage.

Fig. 3 (c) shows the voltage dependence of the surface charge density σ. As seen in Fig. 3 (b), due to the decrease in droplet diameter with increasing applied voltage, the surface charge density continuously increases in all cases. When the droplet charge exceeds the Rayleigh limit (Eq. (1)), the electrostatic force overcomes the surface tension γ_L, thereby causing the droplets to break up, but the charges measured in this study were only up to around 60 to 70% of the Rayleigh limit. In this experimental setup, the electric field is formed between the nozzle and the shield on the Faraday cage, and the droplet is charged by induction within this electric field. Thus, atomization is caused by the downward gravitational and electrostatic forces, which cause the liquid to breakup at a charge of around 60 to 70% of the Rayleigh limit:

$$Q_{\text{Rayleigh}} = 8\pi\sqrt{\gamma_L \varepsilon_0 R^3} \tag{1}$$

where ε_0 is the permittivity of a vacuum (8.85×10^{-12} F m^{-1}), and R is the radius of the droplet.

Since it is important to correlate the charge with the electrostatic force acting on the droplet, we measured the 'electrical surface tension' at the point where the electrostatic and gravitational forces are acting. The electrical surface tension under an applied voltage represents the apparent reduction in the surface tension of the liquid and is essential for analyzing the electrostatic force on a droplet suspended from the nozzle.

For the test equipment shown in Fig. 1, the balance of forces just before the droplet falls is given by

$$\gamma_e = \gamma_L - \alpha\frac{F_g}{\pi D} \tag{2}$$

where γ_e is the electrical surface tension at the point where the electrostatic force is acting, D is the outer diameter of the nozzle, F_g is the gravitational force acting on the droplet, α is a correction coefficient determined from the diameter of the uncharged droplet, and the diameter of the falling droplet is determined by balancing these forces. The electrical surface tension, γ_e, is the difference between the surface tension of

the test liquid γ_L and the gravitational force under an applied voltage and represents the electrostatic force acting on the droplet. In an uncharged state, since there is a balance between the surface tension of the liquid and the gravitational force acting on the droplet just before it falls, the electrical surface tension becomes zero (γ_e=0). If the gravitational force just before the droplet falls is expressed as $(F_g)_0$, the correction coefficient α is given by

$$\alpha = \frac{\gamma_L \pi D}{(F_g)_0} \tag{3}$$

and Eq. (4) is obtained by inputting this into Eq. (2):

$$\gamma_e = \gamma_L \left\{ 1 - \frac{F_g}{(F_g)_0} \right\} \tag{4}$$

Fig. 4 shows the dependence of the dimensionless electrical surface tension on the dimensionless charge. In the figure, pseudo paint refers to a 30:70% (wt%) ethanol/glycerin mixture. The electrical surface tension and the charge are made dimensionless using the surface tension of the liquid γ_L and the Rayleigh limit expressed in Eq. (1), respectively. The electrostatic force acting on the droplet increases with increasing applied voltage as previously described. Since the contribution of the gravitational force F_g decreases with increasing applied voltage, the electrical surface tension asymptotically approaches the surface tension of the test liquid, as expressed in Eq. (4). Therefore, by using the dimensionless electrical surface tension, the breakup condition for the droplets can be regulated independently of the test liquid. From these results, it can be concluded that although physical properties of the liquid such as the surface tension and viscosity influence the droplet charge, they do not significantly influence the electrical surface tension.

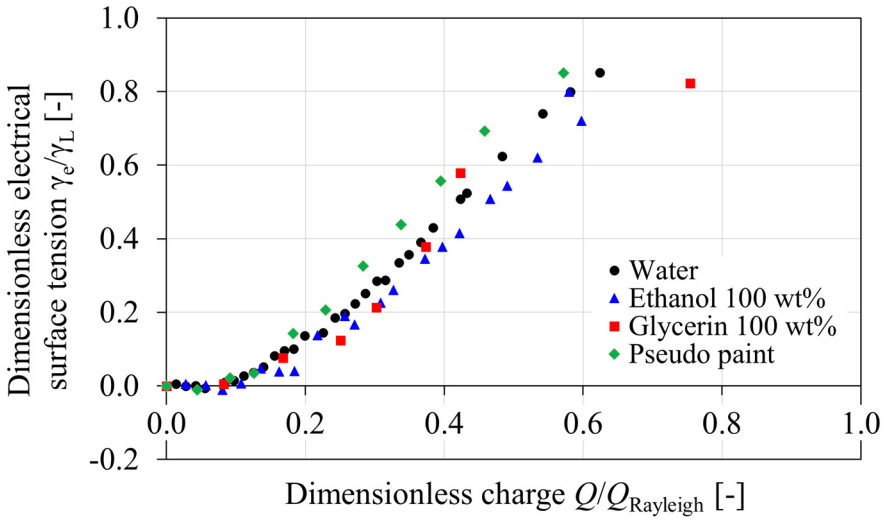

Fig. 4. Dependence of dimensionless electrical surface tension on dimensionless charge.

4. Measurement of surface potential

4.1 Measurement of surface potential for moving droplets

In this study, we assumed that the sensor did not have a finite area but was represented by a single point P, as shown in Fig. 2 (b), and only the surface of the liquid droplet is charged. From Gauss's Law [19], the surface potential at a distance r is given by

$$V = \frac{\sigma}{\varepsilon_0} \frac{R^2}{r} \tag{5}$$

where σ is the surface charge density for the droplet. Substituting R for r in Eq. (5), the surface potential of a droplet V_s is given by

$$V_s = \frac{\sigma R}{\varepsilon_0} \tag{6}$$

As described previously, in preliminary tests we attempted to measure the surface potential of moving droplets but due to the influence of their size and velocity, the values displayed by the sensor were about 1/16th of the applied voltage. We therefore measured the surface potential of initially stationary metallic disks and spheres to investigate the influence of the dimensions and shape of the objects under measurement.

4.2 Correction tests using a disk

4.2.1 Analysis based on electrostatic sensor principles

The electrostatic sensor calculates the surface potential by detecting the electric field at the sensor P in Fig. 2 (b). The electric field $E_{0,c}$ produced by the charged calibration disk (radius $r=b_0$, specified distance d_0) is expressed as:

$$E_{0,c} = \frac{\sigma}{2\varepsilon_0}\left(1 - \frac{d_0}{\sqrt{{d_0}^2+{b_0}^2}}\right) \tag{7}$$

and the surface potential of the disk is

$$V_{0,c} = \frac{\sigma b_0}{2\varepsilon_0} \tag{8}$$

The ratio of $V_{0,c}$ to $E_{0,c}$ is then given by

$$C = \frac{V_{0,c}}{E_{0,c}} = \frac{b_0}{1-\frac{d_0}{\sqrt{{d_0}^2+{b_0}^2}}} \tag{9}$$

If the b_0 and d_0 are considered to be constant, then C is a constant for the electrostatic sensor used in this study. Substituting $d_0 = 10$ mm and $b_0 = 10$ mm, the sensor constant becomes 34.14. Then, by multiplying the electric field $E_{0,c}$ at the sensor by the sensor constant C, an expression for the displayed surface potential of the calibration disk $V_{exp.}$ can be derived:

$$V_{exp.} = CE_{0,c} = 34.14E_{0,c} \tag{10}$$

For $b=b_0$ and $d=d_0$, the value displayed by the sensor, $V_{exp.}$, can be considered the true surface potential. However, when measuring disks with arbitrary dimensions, it is necessary to apply corrections for their size. The electric field E_c formed at a distance d from the surface of a disk of radius b, and the surface potential V_c, are given by Eqs. (11) and (12), respectively,

$$E_c = \frac{\sigma}{2\varepsilon_0}\left(1 - \frac{d}{\sqrt{d^2+b^2}}\right) \tag{11}$$

$$V_c = \frac{\sigma b}{2\varepsilon_0} \tag{12}$$

and, if E_c in Eq. (11) is substituted for E_0 in Eq. (10), an expression for the surface potential is obtained as:

$$V_{\text{exp.}} = 34.14\frac{\sigma}{2\varepsilon_0}\left(1 - \frac{d}{\sqrt{d^2+b^2}}\right) \tag{13}$$

However, because the electric field at the sensor differs from that at the calibration disk, it is not the true value. Comparing the true and displayed values of the surface potential leads to:

$$\frac{V_{\text{c}}}{V_{\text{exp.}}} = \frac{b}{34.14\left(1-\frac{d}{\sqrt{d^2+b^2}}\right)} \tag{14}$$

Here, the value of 34.14 in the denominator on the right-hand side represents the sensor constant C, while the term in parentheses acts as a correction factor that accounts for the disk size and measurement distance.

Equation (14) is defined as a correction coefficient incorporating the sensor constant C (=34.14). Using this correction coefficient, the corrected surface potential $V_{\text{mod.}}$ (=V_{c}) for any disk radius b and measurement distance d can be obtained:

$$V_{\text{mod.}} = \frac{b}{34.14\left(1-\frac{d}{\sqrt{d^2+b^2}}\right)} V_{\text{exp.}} \tag{15}$$

4.2.2 Disk test results

Fig. 5 (a) shows the variation of the surface potential with the disk radius b, for a distance of 10 mm between the sensor and the disk surface. The value $V_{\text{exp.}}$ is that displayed by the electrostatic sensor, and $V_{\text{mod.}}$ is the value corrected using Eq. (15) to take account of the size of the disk. The displayed surface potential is seen to increase with increasing disk radius, and when the radius is equal to the calibration disk radius b_0, the reading becomes the true value (applied voltage 500 V). There is good agreement between the corrected surface potential and the true value when the disk radius exceeds b=5 mm, but for smaller disk radii the corrected values are higher than the true values. This is thought to be due to the influence of electric fields generated by the rod behind the disk and the disk edges.

4.3 Correction tests using a sphere

The electric field, E_{sp}, formed at a distance d from a sphere of arbitrary radius R and the surface potential, V_{sp}, are expressed by Eqs. (16) and (17), respectively.

$$E_{\text{sp}} = \frac{\sigma}{\varepsilon_0}\left(\frac{R}{d+R}\right)^2 \tag{16}$$

$$V_{\text{sp}} = \frac{\sigma R}{\varepsilon_0} \tag{17}$$

Considering that the surface potential is determined by multiplying the electric field at the sensor by the sensor constant, an expression for the displayed surface potential $V_{\text{exp.}}$ is obtained when E_{sp} in Eq. (16) is substituted for $E_{0,\text{c}}$ in Eq. (10).

$$V_{\text{exp.}} = 34.14\frac{\sigma}{\varepsilon_0}\left(\frac{R}{d+R}\right)^2 \tag{18}$$

In this study, we used an electrostatic sensor for flat surface measurement, so it was impossible to obtain a true result for a sphere without modification. Therefore, in the same way as for the disk, by taking the ratio of the true and displayed values of the surface potential and multiplying it by the displayed value, we could provisionally calculate the corrected surface potential as:

$$V_{\text{mod.}} = \frac{R}{34.14\left(\frac{R}{d+R}\right)^2} V_{\text{exp.}} \tag{19}$$

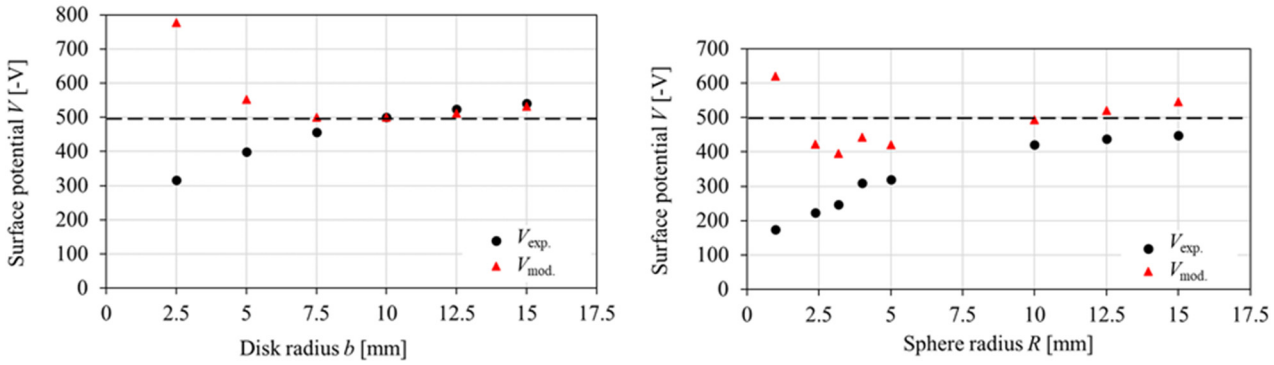

(a) The variation of surface potential with disk radius (b) The variation of surface potential with sphere radius

Fig. 5. The variation of surface potential with disk radius and sphere radius for applied voltage of 500 V.

Fig. 5 (b) shows the variation of the surface potential with the sphere radius R when the distance between the sensor and the sphere surface was 10 mm. The value $V_{\text{exp.}}$ is that displayed by the electrostatic sensor, and $V_{\text{mod.}}$ is the value corrected using Eq. (19) to take account of the shape of the sphere. The displayed surface potential is seen to increase with increasing sphere radius, and when the sphere radius exceeds the equivalent calibration disk radius b_0 ($R \geq b_0 = 10$ mm), it approaches the true value. However, there is a large discrepancy between the two values when the sphere radius is less than 2.5 mm. This is because the correction factor in Eq. (19) has a large value, which is thought to be due to the influence of the electric field generated by the rod behind the sphere. However, since the results for both the disk and the sphere in Fig. 5 show that the corrected values tend to approach the true values, the proposed method can be used to correct for the influence of dimensions and shape.

4.4 Correction of displayed surface potential using regression analysis

In Sections 4.2 and 4.3, we attempted to correct the displayed surface potential for the influence of particle size and dimensions by using the basic principles of the electrostatic sensor. Here we will show the results of a correction method using multi-regression analysis [20, 21]. Multi-regression analysis is a statistical method that links multiple factors and results. A multi-regression equation is created using explanatory variables x_1 to x_n and the result as objective variable Y:

$$Y = b_0 + b_1 x_1 + b_2 x_2 + \ldots + b_n x_n \tag{20}$$

By using this equation, the objective variable Y can be predicted from the explanatory variables x_1 to x_n. It is also possible to investigate which of the explanatory variables x_i have a strong correlation with the objective variable Y. Here, b_i are partial regression coefficients, and indicate the trends in the regression model during multi-regression analysis.

As described earlier, the electrostatic sensor used in this study calculates the surface potential of the object being measured based on the electric field at its sensor. We decided to use the displayed value of the surface potential divided by the applied voltage ($V_{\text{exp.}}/V_{\text{app.}}$) as the objective variable Y, and the sphere radius R and the sphere surface-to-sensor distance d as the explanatory variables x_i. A multi-regression analysis was carried out using the following variables: the metallic sphere radius R, the reciprocal of the sphere surface-sensor distance d, the square of the sphere radius R, the product of the sphere radius R and the reciprocal of the sphere surface-sensor distance d, and the inverse square of the sphere surface-sensor distance d. Using coefficients b_1 to b_5, and segment b_0, the polynomial approximation for the objective variable Y is given by

$$Y = \frac{V_{\text{exp.}}}{V_{\text{app.}}} = b_0 + b_1 R + b_2 \frac{1}{d} + b_3 R^2 + b_4 \frac{R}{d} + b_5 \left(\frac{1}{d}\right)^2 \tag{21}$$

Therefore, it is possible to calculate the corrected surface potential $V_{\text{mod.}}$ if the displayed surface potential $V_{\text{exp.}}$ is divided by the objective variable Y. Using experimental data obtained at an applied voltage of 500 V, the coefficients b_0 to b_5 in Eq. (21) were determined to be:

$$Y=\frac{V_{\text{exp.}}}{V_{\text{app.}}}=0.01111+0.0216R+2.81376\frac{1}{d}-0.007R^2+0.72585\frac{R}{d}-2.491\left(\frac{1}{d}\right)^2 \qquad (22)$$

Fig. 6 shows the dependence of the surface potential on the distance d from the sphere surface to the sensor. Here, $V_{\text{exp.}}$ is the value displayed by the sensor, and $V_{\text{mod.}}$ is the value after correction for the sphere radius and the sphere tip-to-sensor distance using the correction coefficient Y given in Eq. (22). The displayed surface potential increases as the particle size increases and becomes smaller as the distance between the sphere tip and sensor increases. It can be seen that the corrected values $V_{\text{mod.}}$ ($=V_c$) for the surface potential are in good agreement regardless of the sphere size or the sphere surface-to-sensor distance. Although the results shown in Fig. 6 are only for an applied voltage of 500 V, good correlations were also obtained with applied voltages of 1000 V and 1500 V. Even though corrections based on regression analysis have no physical meaning, if the validity of these results can be confirmed, it indicates that accurate measurements of the surface potential may be possible even for small particles.

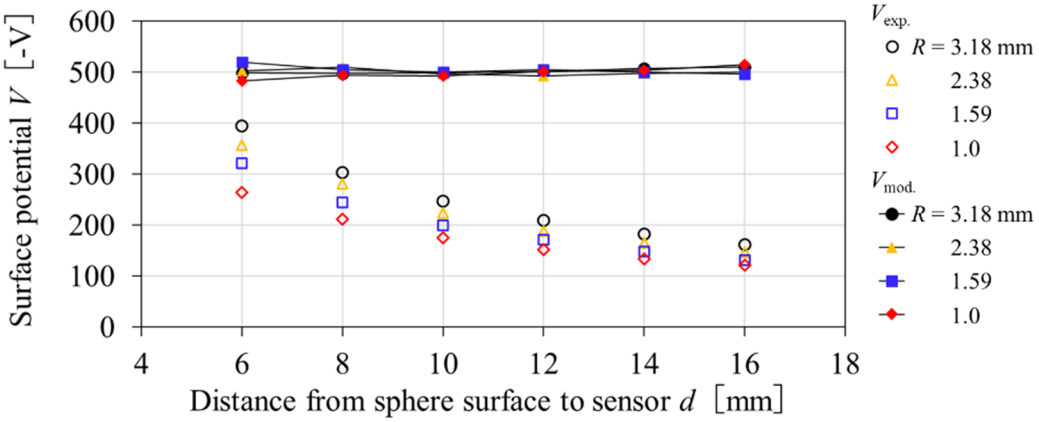

Fig. 6. Dependence of surface potential on distance from sphere surface to sensor for applied voltage of 500 V.

4. Conclusion

The objectives of this study were to investigate the influence of the geometry of a test object on surface potential measurements and to measure the charge and surface potential of liquid droplets in order to clarify the basic characteristics of electrification during spraying.

The main results are as follows:

1. The charge per droplet of liquid initially increases with increasing applied voltage before peaking at a certain voltage and then decreasing due to the generation of satellite droplets and the occurrence of electrical discharge from the edges of the droplets.
2. By making the measured values dimensionless, it was possible to regulate the variation in electrical surface tension with charge, independently of the test liquid.
3. Corrections were made to the surface potential of disks and spheres to take account of the influence of the dimensions and shape of the object being measured, and the corrected values tended to be close to the true values.
4. Corrections for spheres were made by using a multi-regression analysis to give a polynomial approximation for a correction coefficient ($V_{\text{exp.}}/V_{\text{app.}}$). Although this treatment has no physical meaning, the corrected and true surface potentials were in good agreement, regardless of the distance between the sensor and the sphere or the sphere radius.

Acknowledgements

We would like to express our deep appreciation to Professor Yoshiyuki SEIKE of the Faculty of Engineering at Aichi Institute of Technology, Assistant Professor Yusuke KUDO of the College of Industrial Technology at Nihon University, and Dr. Teruo SUZUKI of Kasuga Electric Works Ltd. for their advice on experimental techniques and other matters related to electrostatics during this study.

References

[1] Ogasawara S., Daikoku M., Shirota M., Inamura T., Saito Y., Yasumura K., Shoji M., Aoki H., and Miura T., Liquid atomization using a rotary bell cup atomizer, *J. Fluid Sci. Technol.*, Vol. 5 (3), pp. 464−474, 2010.

[2] Soma T., Katayama T., Tanimoto J., Saito Y., Matsushita Y., H, Aoki, Nakai D., Kitamura G., Miura M., Asakawa T., M. Daikoku, T. Haneda, Hatayama Y., Shirota M., and Inamura T., Liquid film flow on a high speed rotary bell-cup atomizer, *Int.J. Multiphase Flow*, Vol. 70, pp. 96−103, 2015.

[3] Hatayama Y., Haneda T., Shirota M., Inamura T., Daikoku M., Soma T., Saito Y., and Aoki H., Formation and breakup of ligaments from a high speed rotary bell cup atomizer (Part 1: observation and quantitative evaluation of formation and breakup of ligaments), *Proc. Jpn. Soc. Mech. Eng. (B)*, Vol. 79 (802), pp 1081−1094, 2013.

[4] Sawaguchi S., Daikoku M., Himori S., Okabe T., Shirota M., Matsukawa Y., Aoki H., and Fukuno J., Effects of shaping air on breakup of liquid jet, *Proc. 2020 Annual Meeting of the Japan Society of Mechanical Engineers No. 20−1*, 2020.

[5] Matsushita Y. , Katayama T., Saito Y., Matsukawa Y., Okabe T., Shirota M., Inamura T., Daikoku M., Fukuno J., and Aoki H., A Spray painting simulation using high-speed rotary Atomizer-Model development and comparison of LES and RANS-, *Results in Eng.*, Vol. 21, 101697, 2024.

[6] Yasumura K., Saito Y., Shoji M., Matsushita Y., Aoki H., Miura T., Ogasawara S., Daikoku M., Shirota M., and Inamura T., Development of quantitative evaluation method for droplet behavior with high speed rotary bell-cup atomizer, *J. Chem. Eng.*, Vol. 37 (4), pp. 296−304, 2011.

[7] Shirai K., Akiyama Y., Okabe, T. Shirota M., Matsukawa Y., Aoki H., Matsushita Y., Daikoku M., and Fukuno J., Deformation of impacting of electrically charged drops on solid surfaces, *Multiphase flow*, Vol. 36, pp. 353−360, 2022.

[8] Kodama A., Shirai K., T. Miyagawa, T. Okabe, Y. Matsushita, Y. Matsukawa, H. Aoki, M. Daikoku, Y. Saito, J. Fukuno and M. Shirota, Step-wise decrease in contact line velocity of drops impacting a flat smooth surface, *Multiphase flow*, Vol. 37 (2), pp. 226−233, 2023.

[9] Jin R., Daikoku M., Matsukawa Y., Aoki H., Shirota M., Okabe T., Matsushita Y., Miyagawa T., Saito Y., and Fukuno J., The study of breakup and electric characteristics of liquid drop on spray painting, *Proceedings of the 58th Annual Meeting of the Tohoku Branch of the Japan Society of Mechanical Engineers No. 2023-1*, pp. 18−19 The Japan Society of Mechanical Engineers, 2023.

[10] Seike Y., Establishing a technology of electrostatic discharge (ESD) during the environmental-friendly cleansing process of semiconductor devices, *Research Report for FY 2017*, pp. 123-129, The Hibi Science Foundation, 2017.

[11] Tabata Y., Kodama T., and Ohsawa A., Electrostatic charging on liquid caused by spraying, *Specific Research Reports of the National Institute of Industrial Safety*, NIIS-SRR-NO. 17, pp. 59−63, 1999.

[12] Endo Y., Conductivity dependence on spray electrification of flammable solvent, *Safety Eng*, Vol. 59 (3), pp. 175−183, 2020.

[13] Endo Y., Relationship between spray electrification of ethyl acetate and spraying conditions, *Safety Eng.*, Vol. 59 (5), pp. 296−307, 2020.

[14] Japan Alcohol Association, Table of physical properties of ethanol, Ethanol physical properties, etchttps://www.alcohol.jp/sub4.html., last accessed 2025-02-08.

[15] American Cleaning Institute, “PHYSICAL PROPERTIES OF GLYCERINE AND ITS SOLUTIONS”, American Cleaning Institute HP, https://www.cleaninginstitute.org/industry-priorities/science/research/physical-properties-glycerine-and-its-solutions, last accessed 2025-02-08.

[16] Japan Society of Refrigerating and Air Conditioning Engineers, “98 Ultrapure water”, Japan Society of Refrigerating and Air Conditioning Engineers HP, https://www.jsrae.or.jp/annai/yougo/98.html., last accessed 2025-02-08.

[17] HAKKO Corporation, “Flammable Liquids (Electrostatic Precautions)”, HAKKO Corporation HPhttps://eightron.tokyo/inflammable-fluid/., last accessed 2025-02-08.

[18] Lefebvere A.H., and McDonell V.G., Atomization and Sprays (Second Edition), pp. 6−9, CRC Press, 2017.

[19] Y. Kotsuka, [Electromagnetism] Denkijikigaku (in Japanese), p. 48, Morikita Publishing Co., Ltd., 2012.

[20] Ishimura S., and Ishimura K., Introduction to Multivariate Analysis for Beginners, Nyumon Hajimeteno Tahenryokaiseki (in Japanese), pp. 4−7, pp. 34−84, TokyoTosho Co., Ltd., 2019.

[21] Kan T., Introduction to Multivariate Analysis Using Excel, Excel de Manabu Tahenryokaiseki Nyumon, Ohmsha, Ltd., pp. 110−152, 2023. (in Japanese)